Athmarajah, G. *et al.* (2026). *Géotechnique* **76**, No. 4, 579–593 [https://doi.org/10.1680/jgeot.25.00085]

Microwave dry-back of compacted unbound granular materials: an experimental and numerical study

GOPOOJITHAA ATHMARAJAH*, JEFFREY WALKER†, LIUXIN CHEN‡ and JAYANTHA KODIKARA§

After compaction, wet granular pavement layers undergo a dry-back process to remove excess moisture and attain optimal strength and stiffness, and increased performance against cyclic loading. However, the current dry-back method relies on solar radiation, which is time-consuming and weather-dependent, often delaying construction timelines. In this study, the feasibility of microwave drying was investigated as an alternative method to accelerate the dry-back process of compacted unbound granular materials (UGMs). Experimental and numerical analyses were conducted to evaluate the drying behaviour under microwave exposure. The study considered two conditions: direct contact and a 1 cm gap between the microwave applicator and the UGM surface. A three-dimensional finite-element model was developed using COMSOL Multiphysics to simulate the coupled heat and mass transfer, with model validation performed using experimental data. A comparative analysis with solar drying was also conducted using HYDRUS-1D under realistic climatic conditions. The findings demonstrated that microwave drying substantially reduced drying time compared to current dry-back methods while minimising weather-related delays. Despite its efficiency, microwave drying presented challenges such as localised heating and limited energy penetration in deeper layers. The study highlights the potential of microwave technology for pavement dry-back and provides recommendations for optimising microwave drying to enhance energy efficiency in field implementation.

KEYWORDS: microwave processing; moisture-related properties; pavements & roads; temperature

INTRODUCTION

The performance of unbound granular materials (UGMs) is crucial for the structural integrity and durability of road pavements. Achieving optimal performance depends on proper compaction, followed by a dry-back phase that removes excess moisture from the compacted unbound granular pavement layers to enhance the material's strength and stiffness by increasing the suction stress of UGMs (Dutta & Kodikara, 2022; Chen *et al.*, 2024). In road construction, the dry-back process typically aims to reduce the degree of saturation (S_r) to below the relevant limits specified by road authorities, as summarised in Table 1. Traditionally, this process relies heavily on solar drying, which, although widely used and practical, is time-consuming and highly dependent on favourable weather conditions (Athmarajah *et al.*, 2024). Such dependence often delays construction, highlighting the need for faster and more reliable drying techniques in pavement construction.

Microwave drying has emerged as a promising alternative to solar drying, offering the potential for rapid moisture removal. Microwave drying utilises electromagnetic energy to heat the material volumetrically, resulting in a faster drying process (Gulisano & Gallego, 2021; Guo *et al.*, 2021). In civil engineering, microwave energy has been applied to asphalt pavements in various processes, including manufacturing, hot in-place recycling, assisted healing and deicing (Benedetto & Calvi, 2013; Gao *et al.*, 2017; Ding *et al.*, 2018; Flores *et al.*, 2018; Norambuena-Contreras *et al.*, 2018; Zhang *et al.*, 2024). However, the application of microwave energy to accelerate the dry-back process of compacted unbound granular pavement layers has remained unexplored, highlighting a gap in current practice.

The study comprised two key aspects:

(*a*) experimental evaluation of microwave drying performance of compacted UGM, considering critical factors such as temperature distribution, moisture content and the effect of the gap between the antenna aperture and material surface
(*b*) numerical modelling of microwave drying using COMSOL Multiphysics, capturing heat and moisture transfer phenomena and validating the model against experimental data.

A comparative analysis with solar drying was also conducted using HYDRUS-1D simulations under Melbourne climatic conditions to highlight the potential advantages and limitations of the microwave dry-back process in road construction. Consequently, this paper explores the use of microwave technology to dry a compacted UGM, thereby improving the efficiency and effectiveness of the dry-back

Manuscript received 25 February 2025; revised manuscript accepted 12 November 2025.
Discussion on this paper closes six months after article publication; for further details see p. ii.
* ARC Industrial Transformation Research Hub (ITRH) SPARC Hub, Department of Civil and Environmental Engineering, Monash University, Melbourne, Australia (Orcid:0009-0008-8419-7969).
† ARC Industrial Transformation Research Hub (ITRH) SPARC Hub, Department of Civil and Environmental Engineering, Monash University, Melbourne, Australia (Orcid:0000-0002-4817-2712).
‡ ARC Industrial Transformation Research Hub (ITRH) SPARC Hub, Department of Civil and Environmental Engineering, Monash University, Melbourne, Australia (Orcid:0000-0003-0400-8264).
§ ARC Industrial Transformation Research Hub (ITRH) SPARC Hub, Department of Civil and Environmental Engineering, Monash University, Melbourne, Australia (Orcid:0000-0003-1725-7972) (corresponding author: jayantha.kodikara@monash.edu).

Downloaded from http://www.emerald.com/jgeot/article-pdf/76/4/579/11192475/jgeot.25.00085en.pdf by Monash University user on 08 June 2026

Table 1. Relevant limits for dry-back of compacted unbound granular pavement layers

Road agency	Dry-back requirement		Reference
	Parameter	Existing target	
Queensland	Degree of saturation (S_r)	< 60%	Department of Transport and Main Roads Queensland (2021)
New South Wales	Optimum moisture content (OMC)	70%	Transport for NSW (2020)
South Australia	OMC	< 60% (top 20 mm of base layer)	Midgley (2010)
Tasmania	OMC	< 70%	Department of State Growth Tasmanian Government (2014)
Western Australia	OMC	70–85% for gravel; < 60% for crushed rock	Main Roads Western Australia (2021)
Northern Territory	S_r	< 65% for fine crushed rock; 70% for natural gravel	Department of Infrastructure planning and logistics Northern Territory Government (2017)
Victoria	OMC – modified	< 60%	Midgley (2010)
Texas	OMC	2% below the OMC	Texas Department of Transportation (2004)
Florida	OMC	Moisture content of top half of the base < OMC	Florida Department of Transportation (2021)
South Africa	OMC	50%	Hefer & Scullion (2005)

process in pavement construction and developing an optimised microwave drying technique for field applications.

EXPERIMENTAL METHODOLOGY

Material properties and sample preparation

The Class 2 UGM is a typical pavement material used in Australia for base and sub-base layer construction; therefore, it was used in the present study. The particle size distribution was determined using the wet sieving method (AS 1289.3.6.1 (Standards Australia, 2009a), as illustrated in Fig. 1. The geotechnical properties of the selected UGM are outlined in Table 2.

The prepared moist UGMs were compacted separately in two wooden moulds, each measuring 250 mm × 125 mm× 150 mm, as shown in Figs 2(a)–2(c). Metal moulds were not used in the experiments due to their reflective properties with microwave radiation, which pose safety concerns. Furthermore, the size of the wooden moulds was determined based on preliminary numerical simulations to ensure adequate heat dissipation within the compacted UGM sample during microwave drying. A modified compaction rammer was used to compact the material in two layers

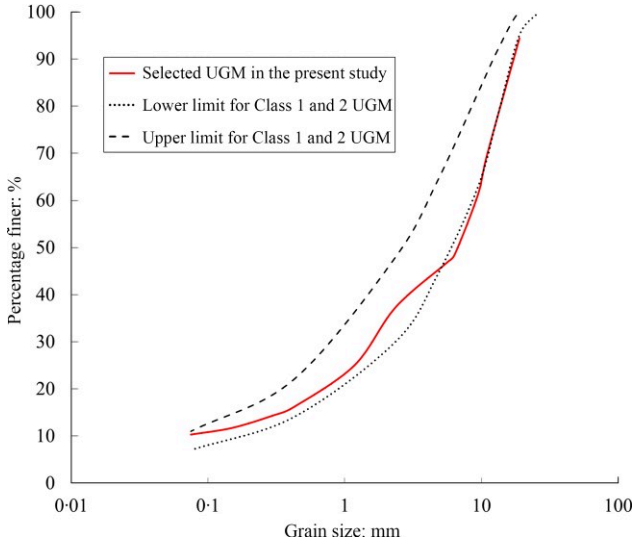

Fig. 1. Particle size distribution of the unbound granular material (UGM) used

within each mould, by applying 300 drops per layer, corresponding to a modified Proctor compaction energy of approximately 2703 kJ/m^3. Following the compaction, the two moulds were combined to form a single sample measuring 250 mm × 250 mm × 150 mm, as shown in Fig. 2(d). This two-mould approach enabled assessment of temperature and moisture variations and allowed a visual inspection of drying extent over the sample depth, particularly at the centre after the microwave dry-back process (Fig. 2(g)). The prepared sample was subsequently subjected to microwave dry-back (Fig. 2(e)). After drying, measurements and observations were conducted on the dried sample to assess the effectiveness of the drying process, as presented in Figs 2(f)–2(g).

Experimental equipment and procedure

A small-scale microwave applicator (Fig. 3) was used for the laboratory experiments to investigate the effectiveness of microwave energy on the dry-back process of compacted UGMs. The set-up consisted of an open structured horn antenna with 110 mm × 55 mm aperture dimensions, which directs the microwave energy to the compacted UGMs. The horn antenna was attached to a waveguide with dimensions 86 mm × 43 mm. A magnetron sourced from a commercial microwave oven operating at 900 W with a frequency of 2·45 GHz was assembled to the launcher to generate microwaves and channel the energy through the horn antenna. A microwave leakage detector (Extech 480846) was used to periodically monitor radiation levels and ensure compliance with the allowable time-averaged exposure to electric fields at 2·45 GHz (137 V/m root mean square (RMS)) as recommended by the Australian Radiation Protection & Safety Agency (2002). The selected microwave power of 900 W corresponds to the maximum rated output of the small-scale microwave applicator used in this study. This power level was chosen to ensure a safe and controlled laboratory operation without excessive radiation exposure or equipment overheating.

The combined UGM sample was dried at different time durations under two distinct conditions: (*a*) direct contact: the antenna aperture was placed directly on the surface of the compacted UGM; and (*b*) gap condition: a 1 cm gap was maintained between the antenna aperture and the surface of the compacted UGM.

The longer edge of the antenna aperture was aligned parallel to the intersection of the two moulds during all experiments to ensure a consistent positioning of the antenna

Downloaded from http://www.emerald.com/jgeot/article-pdf/76/4/579/11192475/jgeot.25.00085en.pdf by Monash University user on 08 June 2026

Table 2. Geotechnical properties of the unbound granular material (UGM) used

Geotechnical property	Value	Relevant standard
Maximum dry density, modified, MDD: kg/m^3	2345	AS-1289.5.2.1 (Standards Australia, 2017)
Optimum moisture content, modified, OMC: %	5·7	AS-1289.5.2.1 (Standards Australia, 2017)
Optimum degree of saturation, $S_{r,opt}$: %	85	AS-1289.5.2.1 (Standards Australia, 2017)
Specific gravity	2·78	AS-1289.3.5.1 (Standards Australia, 2006)
Liquid limit, LL: %	22	AS-1289.3.1.1 (Standards Australia, 2009b)
Plastic limit, PL: %	17·5	AS-1289.3.1.1 (Standards Australia, 2009b)
Plastic index, PI: %	4·5	AS-1289.3.1.1 (Standards Australia, 2009b)
Fine percentage: %	10·4	AS-1289.3.6.1 (Standards Australia, 2009a)

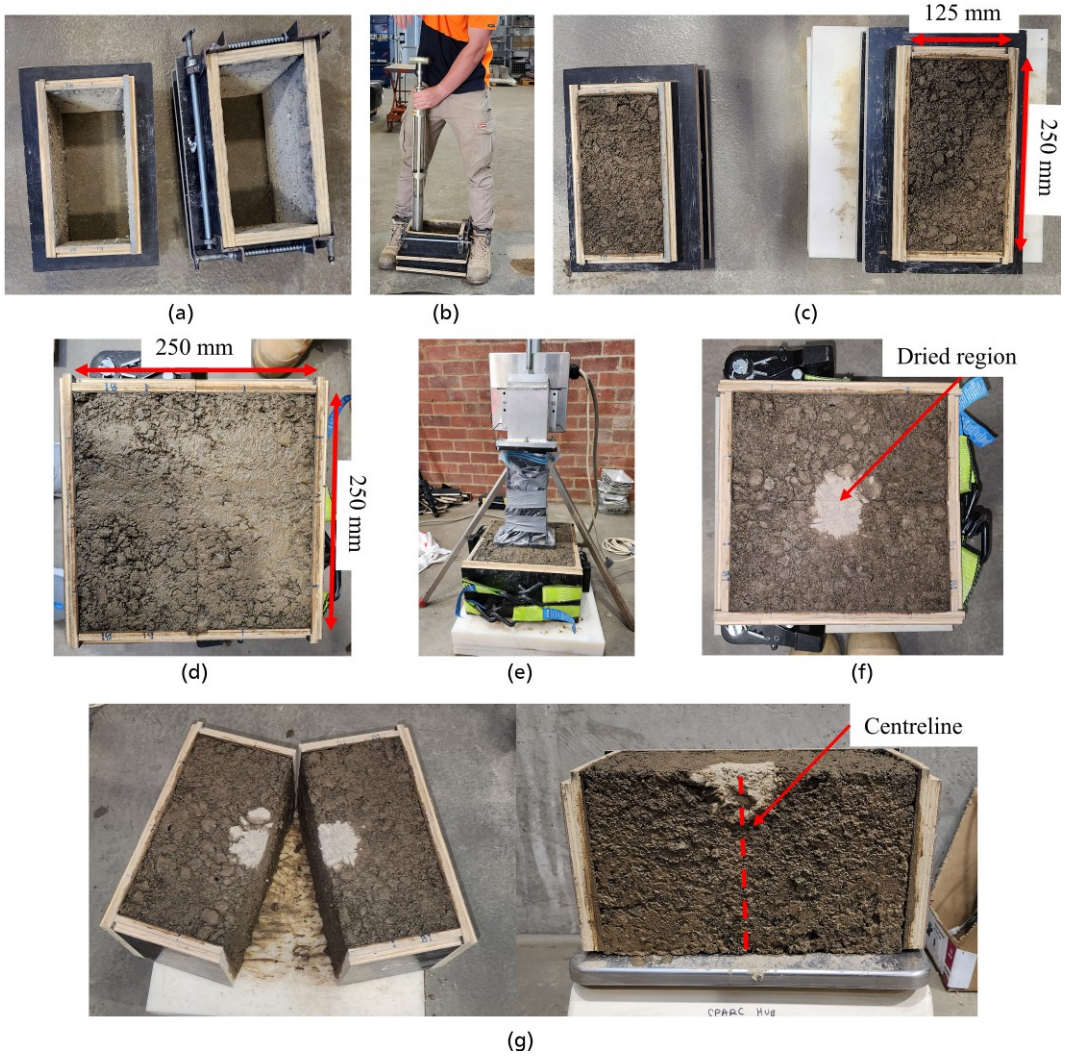

Fig. 2. Experimental stages: (a) two empty wooden moulds; (b) compaction of UGMs; (c) compacted UGMs in two wooden moulds; (d) combined UGM sample; (e) microwave drying of compacted UGM sample; (f) UGM sample after microwave drying; and (g) split UGM sample for data collection

relative to the compacted UGM sample, thus minimising potential variations in the results due to alignment differences. After each drying process, infrared (IR) thermal images were captured using a thermal imaging camera (FLIR B200). Thermal images were taken immediately after microwave drying to minimise the exposure time of the samples to the environment. The IR images were then post-processed in MATLAB to evaluate surface temperature variations and generate consistent contour maps. To determine the moisture content variations after microwave drying, the combined sample was separated, and core samples representing ~20 mm × 40 mm of material were manually collected at 50 mm intervals along the centreline of the compacted UGM (Fig. 2(g)). Given the low fine content and the minimal shrinkage or expansion typically observed in UGMs, the initial dry density was assumed constant when calculating the degree of saturation (S_r), as

$$S_r = \frac{w \times G_s}{e}, \tag{1}$$

$$e = \frac{\rho_w \times G_s}{\rho_d} - 1 \tag{2}$$

where w is the gravimetric moisture content; G_s is the specific gravity; e is the void ratio; ρ_w is the density of water

Downloaded from http://www.emerald.com/jgeot/article-pdf/76/4/579/11192475/jgeot.25.00085en.pdf by Monash University user on 08 June 2026

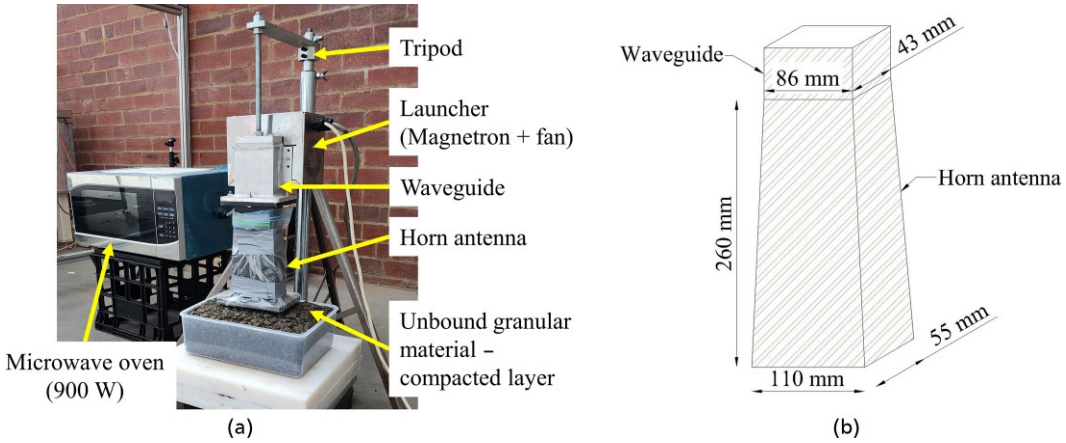

Fig. 3. (a) Small-scale microwave applicator used for microwave dry-back experiments of compacted UGMs and (b) schematic diagram of the waveguide and horn antenna arrangement

(=1000 kg/m^3); and ρ_d is the dry density. The assumption of constant dry density is supported by the UGM's low plasticity (PI = 4·5%) and is consistent with Austroads (2008), Department of Transport and Main Roads Queensland (2021) and VicRoads (2017), which note that UGMs with low plasticity indices exhibit negligible shrink–swell behaviour.

A summary of different drying durations and initial conditions for each sample, including the moisture content, dry density and S_r, is outlined in Table 3. To replicate field compaction practices, where UGMs are compacted near their optimum moisture content (OMC) to achieve maximum dry density (MDD) with minimal compaction effort (Tophel *et al.*, 2022), samples were prepared at moisture contents in the range from 5·5 to 6%, closely aligning with the OMC of 5·7% determined under modified compaction conditions. Since compaction near the OMC typically results in S_r between 80 and 90%, the selected initial S_r range is appropriate for evaluating the dry-back behaviour of compacted UGMs under microwave energy. It is important to note that each experiment involved separately prepared and compacted UGM samples, resulting in slight variations in initial conditions.

The microwave drying process produced a distinct drying region on the surface of the compacted UGM, approximated by an ellipse, as shown in Fig. 4(a). The dried region extended into the sample, forming a semi-ellipsoid (Fig. 4(b)). The dimensions of the dried region on the surface (A), as well as the total dried volume (V), were quantified using three key parameters: the length of the major axis (a), the length of the minor axis (b) and the depth (h). This geometric representation was adopted as a practical approximation of the irregular dried region, providing a quick and consistent method for calculating the

Table 3. Initial conditions of compacted UGM samples used in microwave dry-back experiments

Experimental condition	Sample	Drying time: min	Initial gravimetric moisture content: %	Dry density: kg/m^3	Initial S_r: %
Direct contact	S1	3	5·76	2342·4	85·7
	S2	4	5·82	2342·7	86·7
	S3	5	5·79	2346·7	87·2
Gap condition	S4	3	5·74	2360·7	89·9
	S5	4	5·59	2370·4	90·0
	S6	5	5·75	2345·9	86·4

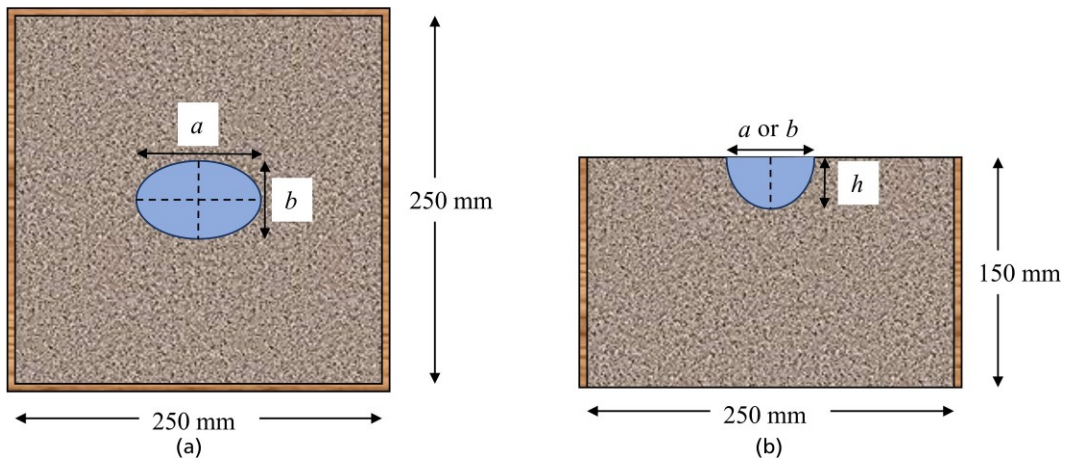

Fig. 4. Schematic diagram of the shape of the dried region after microwave drying: (a) surface view; (b) cross-section along the depth

Downloaded from http://www.emerald.com/jgeot/article-pdf/76/4/579/11192475/jgeot.25.00085en.pdf by Monash University user on 08 June 2026

dried area and volume across different test conditions. It is also noted that this representation is a simplification of the true irregular boundary and may lead to deviations when the dried patch is asymmetric.

Numerical model development

To investigate the drying process of compacted wet UGMs using a small-scale microwave applicator, a three-dimensional (3D) finite-element model was developed using COMSOL Multiphysics. This model couples the interdependent physics of electromagnetic wave propagation, heat transfer and moisture transport within an unsaturated porous medium. The intricate coupling of these processes, which depends on spatial and temporal variations, posed substantial challenges requiring innovative modelling techniques and considerable computational effort.

Figure 5 illustrates the geometry and finite-element mesh of the model. The computational domain was discretised using tetrahedral elements. A quadratic shape function was employed in the numerical simulations. A user-controlled mesh was generated, where element sizes were defined based on the domain regions. Specifically, the horn antenna was assigned an extra fine mesh with a maximum element size of 0·02 m. The air gap and UGM domains were assigned an extremely fine mesh, with a maximum element size of 0·0114 m, to resolve the energy distribution and heat transfer processes within the granular materials. The overall mesh consisted of 192 703 tetrahedral elements, 10 294 triangular elements and 24 vertex elements, with 34 220 mesh vertices. The average element quality was 0·6626, ensuring a well-conditioned mesh for numerical stability (Li *et al.*, 2019).

The transmission of microwave energy from the magnetron to the compacted UGM was facilitated by a rectangular waveguide operating in the TE10 mode. To simulate the gap condition, the designated finite elements were assigned air properties, ensuring physical continuity in the model. This consideration allowed for accurate wave propagation, energy dissipation and convective heat transfer at the surface, replicating actual experimental conditions. The initial conditions were assigned based on laboratory measurements, while the boundary conditions accounted for convective heat and moisture exchange at exposed surfaces. Further details on model development, underlying assumptions, governing equations, parameter values and boundary formulations are provided in the online supplementary material.

RESULTS AND DISCUSSION

Comparison of experimental and numerical results

Direct contact. The comparison between variations in S_r along the depth of the compacted UGM sample and the rise in the surface temperature after 3 min of drying, obtained from both laboratory experiments and numerical simulations, is presented in Fig. 6. Key statistical metrics including the coefficient of determination (R^2), mean absolute error (MAE) and root mean square error (RMSE) were calculated to evaluate the model accuracy. It should also be noted that the moisture content/S_r measurements during laboratory experiments were carried out for the volume of samples at different depth intervals. In contrast, the numerical model compares the S_r variations along the centreline of the compacted UGM depth, which may have contributed to differences between experimental and simulated values.

The experimental and numerical model data in Fig. 6 demonstrate that the developed model reasonably predicts the drying behaviour of compacted UGM during microwave drying. Notably, there is a slight discrepancy between the simulated and measured S_r near the surface of the compacted UGM. This discrepancy might be attributed to modelling simplifications, such as the assumption of uniform material properties and idealised boundary conditions. In addition, the manual positioning of the antenna and the data collection process could inherently introduce some degree of uncertainty, which is unavoidable in practical experimental set-ups. Nonetheless, the model effectively captured the overall variation of S_r, with R^2 value of 0·892 and RMSE of 6·2%, indicating a good agreement between the numerical and experimental datasets. In addition, the rise in surface temperature in numerical simulations shows a close match with the measured surface temperature, as illustrated in Fig. 6(b). Furthermore, surface temperature variations along the two centrelines of the material (axes A and B as shown in Fig. 6(b)) are depicted in Figs 6(c) and 6(d). The measured and simulated profiles exhibit similar peak temperatures and radial decay patterns along both axes, indicating that the model captures the spatial distribution of microwave-induced heating across the sample surface.

Further analyses were carried out for different drying durations, as depicted in Fig. 7, to validate the developed numerical model. The developed 3D numerical model reasonably captured the distribution of S_r and surface temperature after 4 and 5 min of microwave drying (Fig. 7). Interestingly, the prediction accuracy of the developed model improved with extended drying durations, with R^2

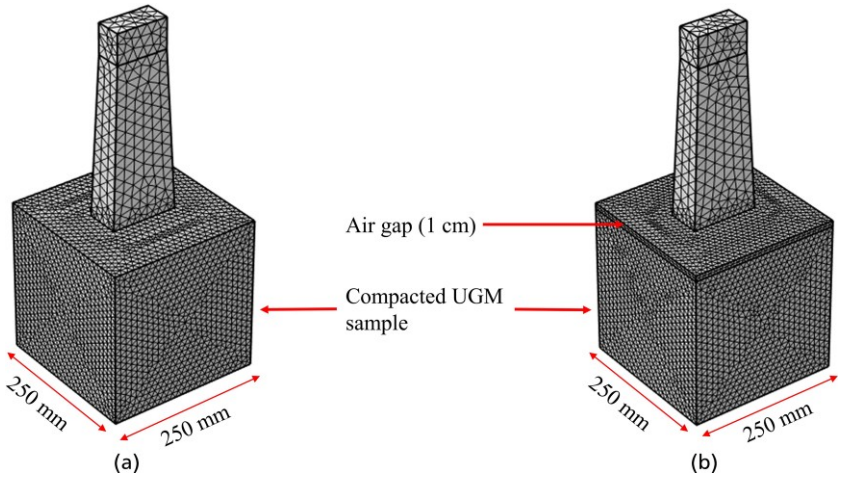

Fig. 5. Geometric representation and meshing of the model: (a) direct contact condition; (b) gap condition

Downloaded from http://www.emerald.com/jgeot/article-pdf/76/4/579/11192475/jgeot.25.00085en.pdf by Monash University user on 08 June 2026

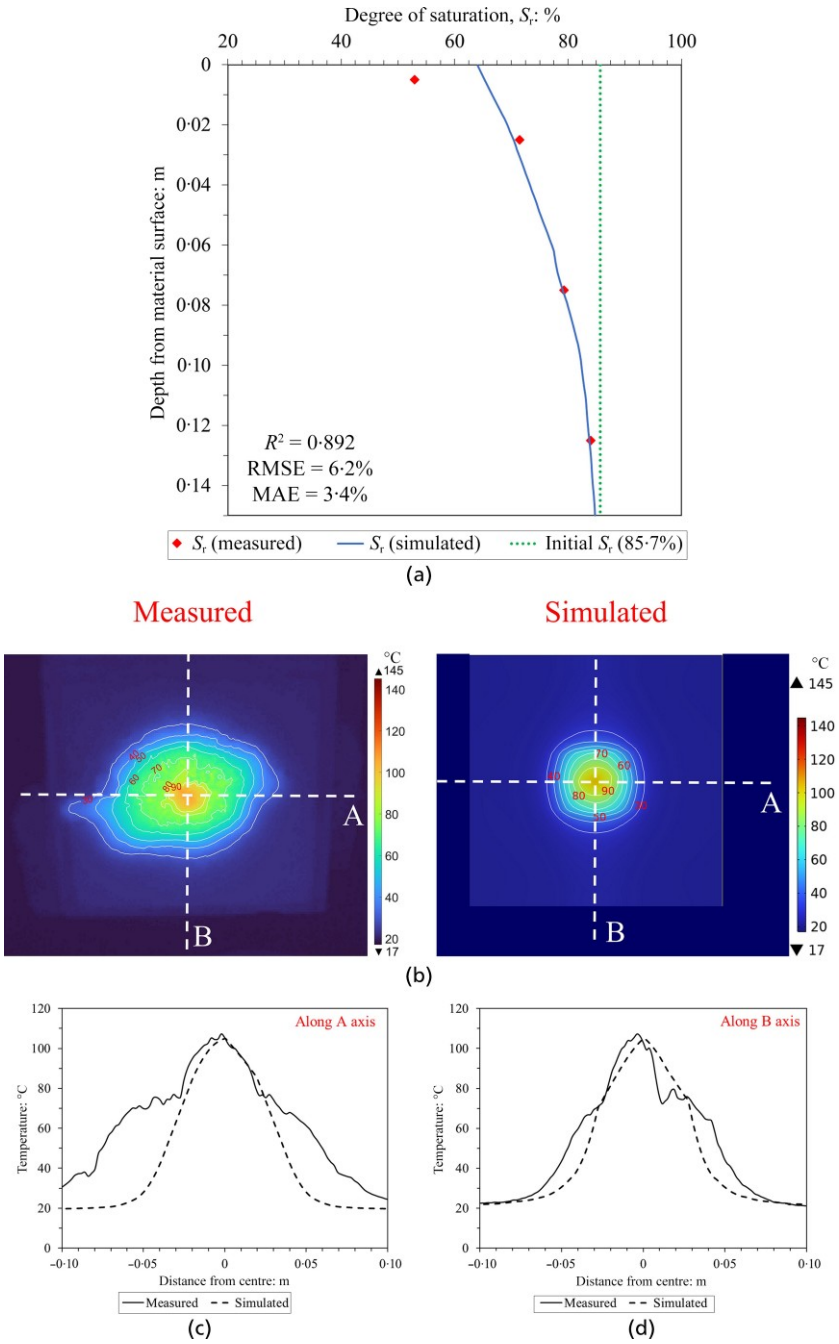

Fig. 6. Comparison of experimental and numerical results after 3 min of microwave drying: (a) variation of the degree of saturation (S_r); (b) measured and simulated surface temperature; (c) surface temperature variation along axis A; and (d) surface temperature variation along axis B

values of 0·911 and 0·972 for 4 and 5 min of drying, respectively. In addition, the predicted surface temperature distributions depicted in Fig. 7(c) closely matched the measured temperatures (Fig. 7(b)) for both drying durations. Furthermore, measured and simulated surface temperatures showed a progressive rise in maximum surface temperatures with increasing drying times. This indicates that longer drying times facilitated more absorption and conversion of microwave energy into heat within the compacted UGM sample.

Interestingly, the surface temperature distribution observed in the IR thermal images (Fig. 7(b)) exhibited a distinct elongated pattern. This localised effect can be attributed to the energy distribution at the UGM surface. Numerical simulations provided additional insights into the power intensity distribution at the material surface, as shown in Fig. 8, revealing that the maximum power intensity was concentrated at the centre of the antenna aperture and decreased radially outward from the centre, particularly along the longer edge of the aperture. This asymmetric power or energy distribution aligns with the observed temperature variations, indicating its critical role in the drying process and its potential to cause localised drying.

Khan *et al.* (2018) reported a similar distribution pattern in a similar-sized antenna, with maximum intensity concentrated at the centre of the antenna and significant intensity extending about two-thirds of the length along the longer aperture edge. The asymmetric power distribution along the aperture axis observed in numerical simulations aligns with these findings and further supports the observations during laboratory experiments. However, the simulated surface temperatures (Fig. 7(c)) did not reproduce the

Downloaded from http://www.emerald.com/jgeot/article-pdf/76/4/579/11192475/jgeot.25.00085en.pdf by Monash University user on 08 June 2026

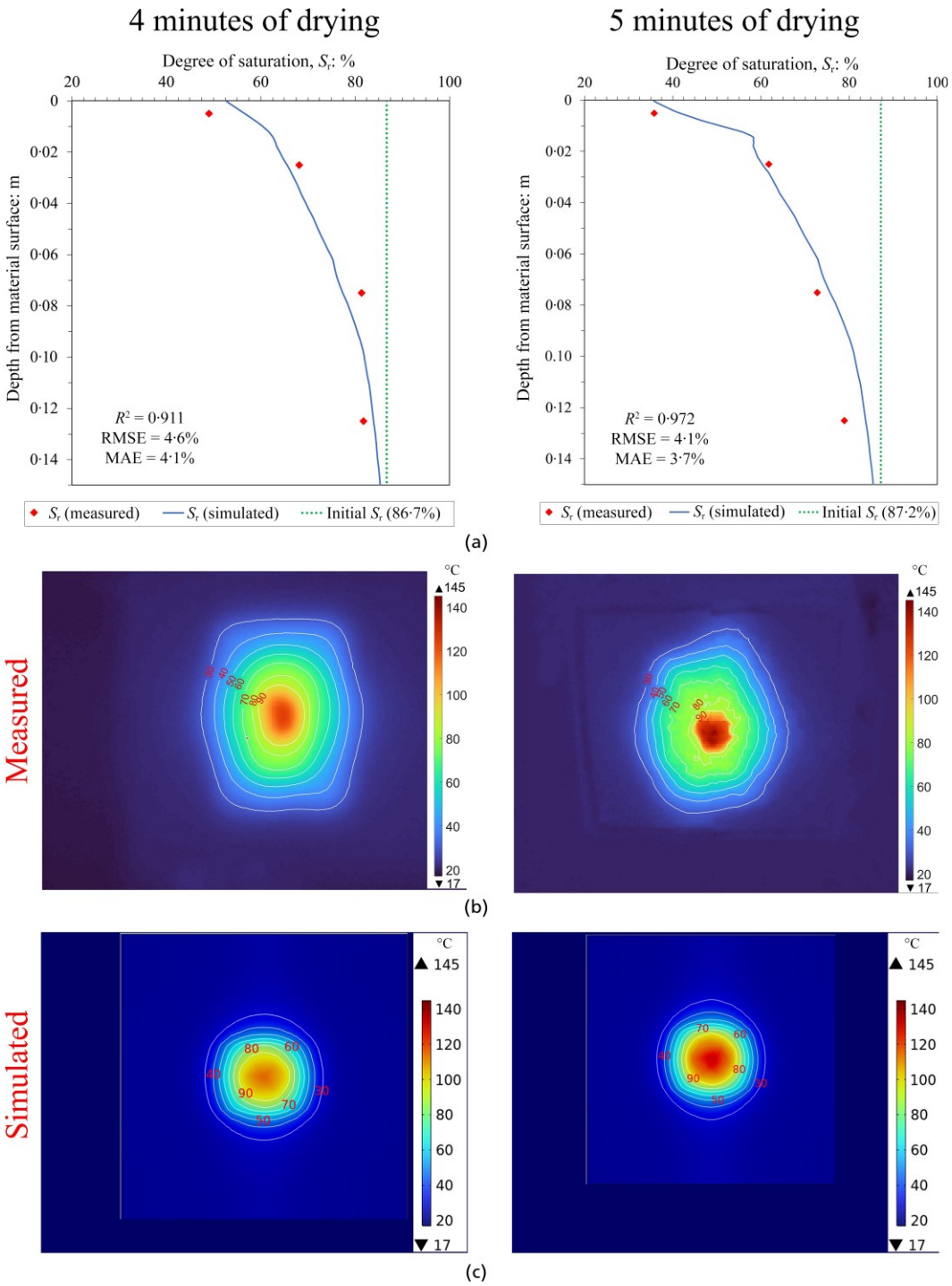

Fig. 7. Variation of S_r and surface temperature distribution obtained from experiments and numerical simulations at different drying durations: (a) S_r variation; (b) surface temperature measured and post-processed in MATLAB; and (c) surface temperature simulated in COMSOL

elongated shape observed in the IR images; instead, they showed a more symmetric pattern. This discrepancy could arise from certain experimental realities that were not incorporated into the numerical model. For instance, the antenna aperture was covered with a protective bag during experiments, as shown in Fig. 2(e), to minimise potential damage to the magnetron from vapour intrusion. This bag, which was not accounted for in the numerical modelling, may have influenced the heat transfer at the material surface, potentially enhancing localised conduction and contributing to the elongated temperature patterns.

In addition, the surface of the sample was not perfectly smooth or even, as shown in Fig. 2, which could have caused slight misalignments of the antenna during experiments. In contrast, the numerical simulations assumed a smooth surface and direct antenna–material interface, which was likely to have over-simplified the actual conditions and contributed to the observed differences. Incorporating these experimental factors, such as the influence of the protective bag, surface irregularities and potential antenna misalignments, into simulations could enhance the model's predictive accuracy.

Figure 9 illustrates the comparison of the visible dried region on the surface and along the depth at different drying durations. The dried area on the surface expanded progressively with longer drying times, as seen in Fig. 9(a). This expansion suggests that while the drying was initially

Downloaded from http://www.emerald.com/jgeot/article-pdf/76/4/579/11192475/jgeot.25.00085en.pdf by Monash University user on 08 June 2026

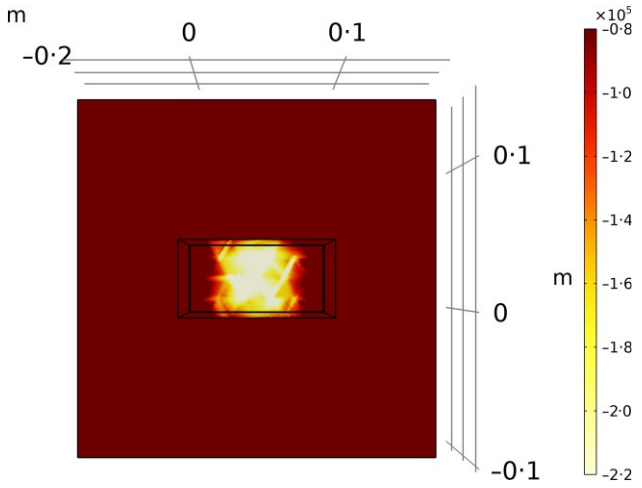

Fig. 8. Power intensity (W/m^2) at the surface of the compacted UGMs exposed to microwave radiation for 5 min. Negative values indicate the direction of the microwave energy or power flow, representing energy absorption into the UGM sample

concentrated in a smaller area, heat distribution during extended drying duration eventually caused a slight expansion of the visibly dried region on the sample surface. However, it can be observed that the dried region after 4 min of drying showed a slight drop compared to the area observed after 3 min of drying. This observed reduction may be attributed to a combination of factors, including the non-uniform distribution of initial moisture within the compacted UGM samples, possible misalignment of the antenna during experiments, or environmental factors such as airflow or varying ambient temperature might have influenced the surface drying of the compacted UGM samples at different drying durations.

The sectional images of the UGM samples shown in Fig. 9(b) revealed that the depth of the visible dried region extended progressively with increased drying time, indicating a deeper penetration of microwave energy within the compacted material. Furthermore, this observation could be attributed to changes in the relative complex permittivity of UGM during the microwave drying process. It was observed in a study by the current author (Athmarajah *et al.*, 2025) that the dielectric constant and dielectric loss of the selected UGMs decrease with increasing temperature, leading to deeper penetration of microwave energy at higher temperatures. Overall, the growing area and depth of the visible dried region resulted in an increase in dried volume with extended drying periods (Fig. 9). Furthermore, these observations aligned with the trends observed in the numerical simulations, where extended drying durations resulted in deeper penetration of microwave energy, leading to greater overall drying efficiency.

The observed variations in S_r (Figs 6(a) and 7(a)) indicate that the microwave dry-back process of compacted UGMs lacks uniformity over the depth of the compacted UGM sample. Another notable limitation of these laboratory experiments is their departure from real-world conditions. In practice, microwave applicators or horn antennas mounted on moving vehicles cannot be placed directly on the surface of the compacted UGM layer due to the risk of damaging the pavement layers. Hence, a consistent gap of 1 cm was maintained between the antenna aperture and the surface of the compacted UGM layer for the next set of experiments to replicate actual field applications and ensure the validity and applicability of findings.

Gap condition. The variation of S_r along the depth of the compacted UGM sample for the experiments conducted with a 1 cm gap between the antenna aperture and sample surface across different drying durations is depicted in Fig. 10. The results demonstrate a progressive decrease in S_r with increasing drying time, as observed in the experiments with the antenna placed on the surface of the compacted UGM sample. This observation indicates that the moisture removal rate and drying uniformity vary with the drying duration.

Deviations in predicted and measured S_r, specifically during shorter durations, may be attributed to the initial experimental conditions and potential experimental errors, as discussed previously. In addition, the assumption of constant gas pressure in the model may have contributed to these discrepancies. In reality, elevated temperatures increase not only vapour pressure but also dry air pressure,

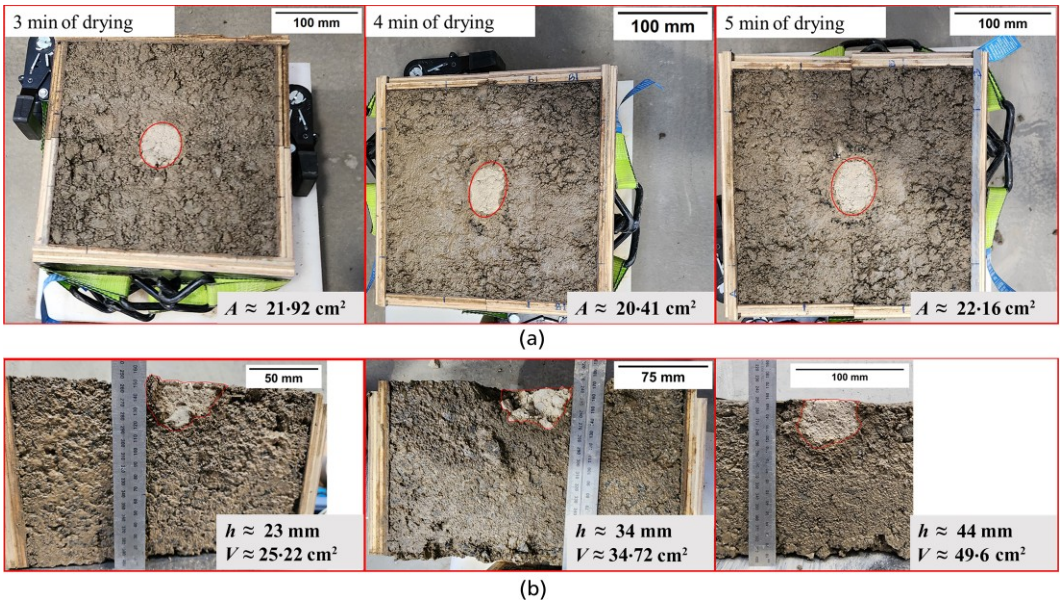

Fig. 9. Comparison of drying efficiency of compacted UGM samples at different drying durations during the experiments with the antenna placed on the surface of material: (a) visible dried region on the surface; (b) visible dried region along the depth

Downloaded from http://www.emerald.com/jgeot/article-pdf/76/4/579/11192475/jgeot.25.00085en.pdf by Monash University user on 08 June 2026

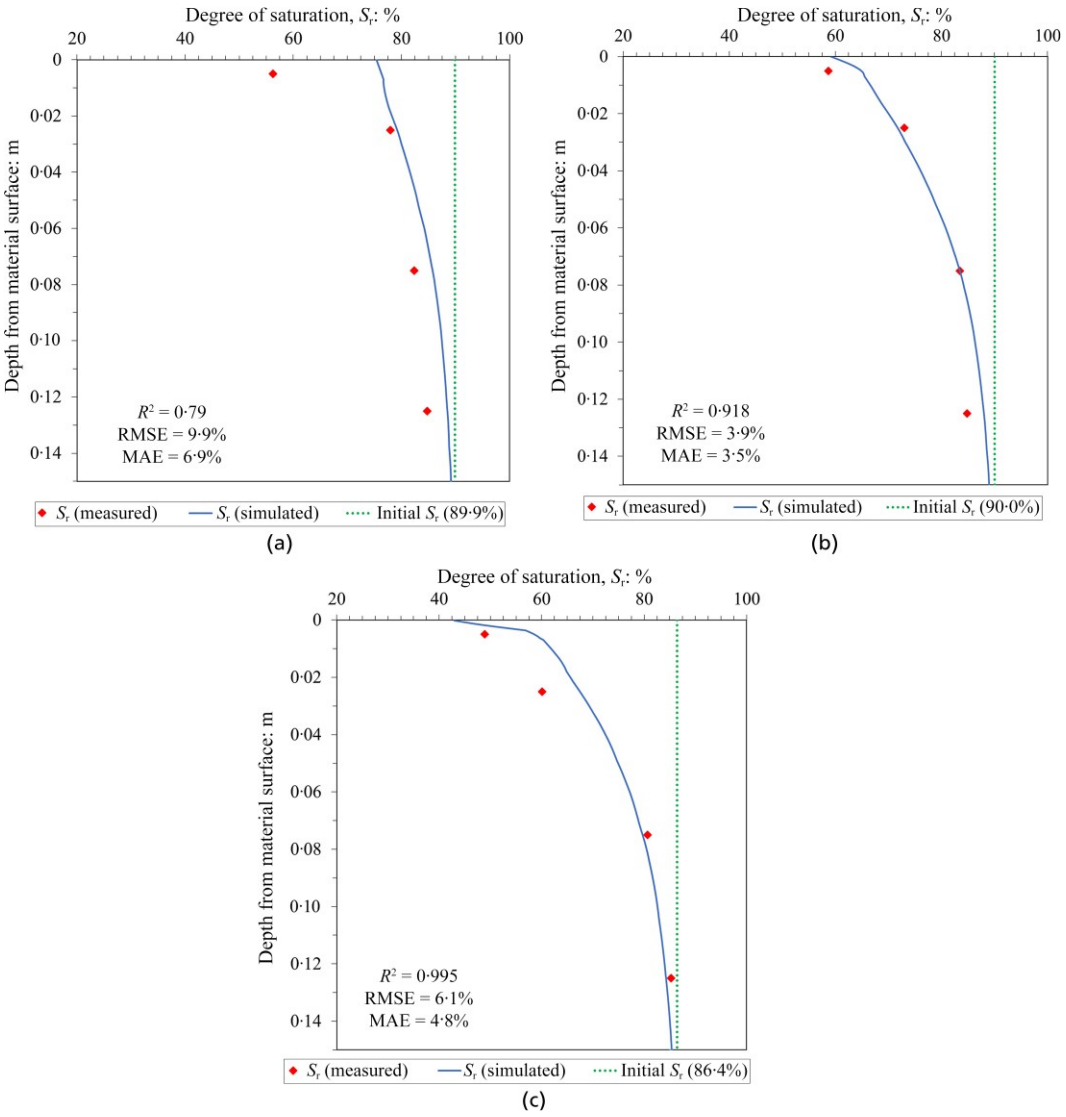

Fig. 10. Variation of S_r for the experiments carried out with a 1 cm gap between the antenna aperture and compacted UGM surface: (a) after 3 min of drying; (b) after 4 min of drying; and (c) after 5 min of drying

which affects suction and coupled moisture transfer within the porous medium (Jahangir & Sadrnejad, 2013). Since this effect was not captured in the current model, it may partly explain the differences observed between experimental and simulated results. Moreover, the soil water retention curve (SWRC) used in the simulations was measured at room temperature (≈ 20°C) and the potential influence of temperature on the SWRC was not incorporated. This simplification may also have contributed to the deviations observed. Nevertheless, the developed model captured the variation of S_r well within the compacted UGM sample, as shown in Figs 6(a), 7(a) and 10. The incorporation of temperature-dependent SWRC and variable gas pressure in future simulations could further enhance predictive accuracy.

The surface temperature distribution observed during the microwave drying process with a 1 cm gap between the aperture and sample surface is presented in Fig. 11. IR thermal images captured during the laboratory experiments (Fig. 11(a)) are compared with the simulated surface temperature distributions obtained from COMSOL Multiphysics after different drying durations (Fig. 11(b)). The comparison indicates that the model provides a reliable prediction of surface temperature distribution under gap conditions.

The rise in surface temperatures was observed to be notably lower under the gap condition, specifically at extended drying durations (Fig. 11), compared with the direct contact condition (Figs 6(b), 7(b) and 7(c)). This result suggests that a gap between the antenna and material surface leads to a reduction in electric field strength (Brodie & Hollins, 2015), resulting in reduced energy absorption and heat generation at the surface of the compacted UGM sample.

Figure 12 shows the drying behaviour of the compacted UGM samples at different drying durations during experiments with a 1 cm gap maintained between the antenna aperture and the material surface. The observed area and depth of the visible dried region exhibited a similar increasing trend with drying duration, as seen in the direct contact experiments (Fig. 9). A comparison of the visible dried regions on the surface between the two experimental conditions revealed that the area of dried regions showed minimal differences at a given drying duration (Figs 12(a) and 9(a)). However, the observed depth of drying was comparatively higher during longer drying times (4 and 5 min of microwave drying) in the direct contact experiments. It is noteworthy that the microwave dry-back process of compacted UGM samples is primarily based on a temperature-driven moisture diffusion process (Athmarajah *et al.*, 2024). Therefore, higher temperatures may facilitate more drying of the compacted UGM sample, resulting in a greater depth of drying. Moreover, the effect of varying temperatures on the relative complex

Downloaded from http://www.emerald.com/jgeot/article-pdf/76/4/579/11192475/jgeot.25.00085en.pdf by Monash University user on 08 June 2026

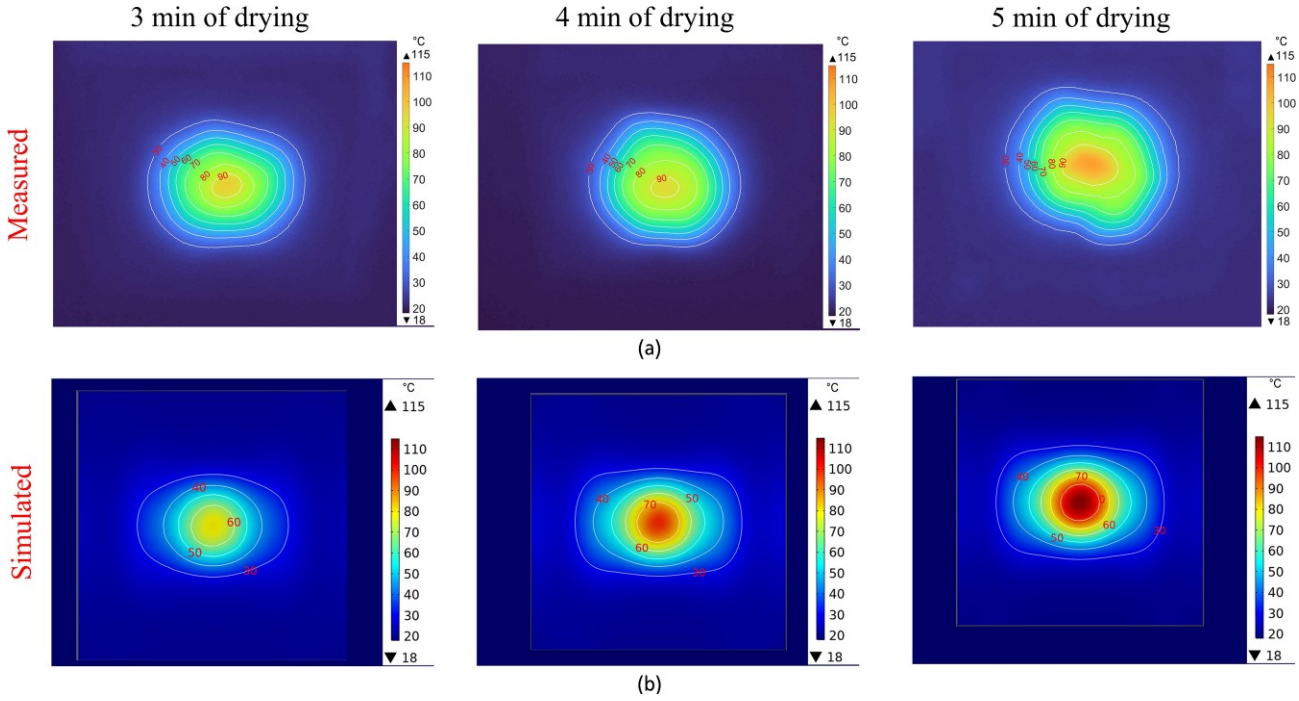

Fig. 11. Variation of surface temperature for the experiments conducted with 1 cm gap: (a) infrared (IR) thermal images post-processed in MATLAB; (b) simulated surface temperature

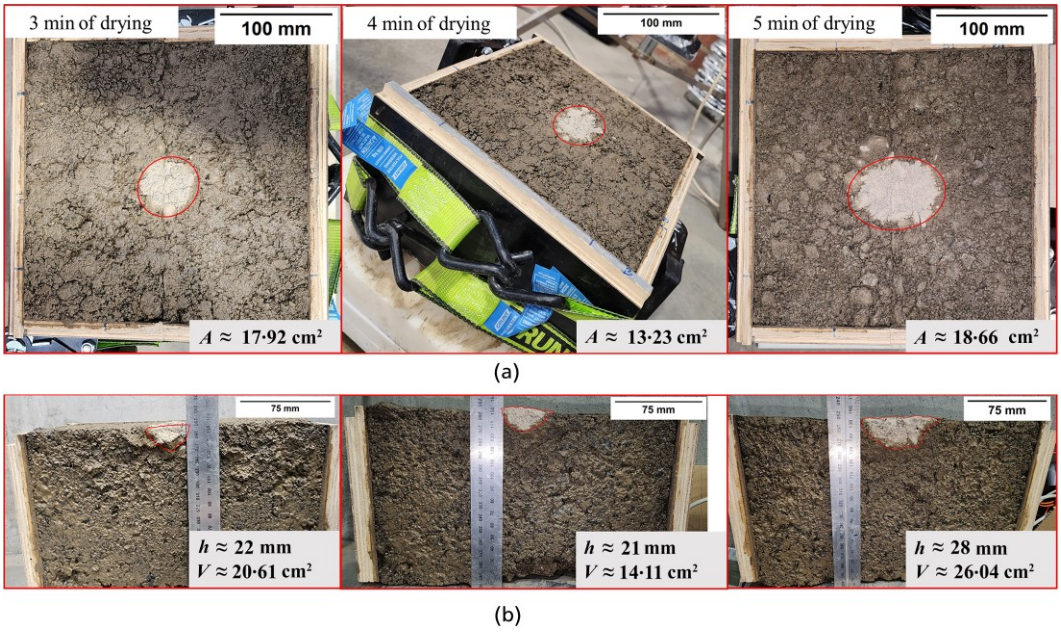

Fig. 12. Comparison of drying efficiency of compacted UGM samples at different drying durations during the experiments with a 1 cm gap: (a) visible dried region on the surface; (b) visible dried region along the depth

permittivity of UGM may result in reduced penetration of microwave energy when a gap is maintained, which could lead to a reduced depth of moisture removal. Overall, the smaller area of the dried region and the depth of significant drying under gap conditions resulted in a smaller volume of dried sample compared to direct contact conditions.

Comparison of microwave and solar drying through numerical simulations

The efficiency of the dry-back process of compacted unbound granular layers plays a critical role in the timely completion of pavement construction projects. Comparing microwave and solar drying under controlled conditions allows evaluation of their relative advantages and limitations and the feasibility of microwave drying for real-world applications.

Numerical simulations for microwave drying and solar drying were performed using validated numerical models, with the results compared in this section. The solar drying was simulated using HYDRUS-1D, while the microwave drying was modelled using COMSOL Multiphysics. The governing equations and the development of the numerical model for solar drying were detailed in previous works by Athmarajah *et al.* (2023) and Athmarajah (2025).

The solar drying model was a one-dimensional (1D) simulation with a domain length identical to that used in the

Downloaded from http://www.emerald.com/jgeot/article-pdf/76/4/579/11192475/jgeot.25.00085en.pdf by Monash University user on 08 June 2026

microwave drying model (150 mm) to ensure consistency in the analyses. Furthermore, Melbourne's climatic data was chosen for solar drying analysis, as Melbourne was the location for the microwave drying experiments, which provided realistic and consistent comparisons. The same climatic dataset for the year 2022, as previously used in the study by Athmarajah (2025), was utilised for this analysis. January was chosen to represent summer conditions, characterised by high ambient temperatures and evaporation rates, while July was selected to represent winter conditions with lower temperatures and evaporation rates. In addition, the boundary conditions for solar drying were the same as those used in the previous study by Athmarajah (2025).

For microwave drying, simulations were carried out for short durations (up to 5 min), therefore, the average values of ambient temperature, relative humidity and wind speed for the selected summer and winter periods were used as boundary conditions in COMSOL. The variations of Melbourne's climatic conditions for the specified periods are presented in Figs 13 and 14, with the average wind speeds during these periods being 17·5 km/h in summer and 17·2 km/h in winter, as recorded from Australian Bureau of Meteorology data.

The initial conditions of the compacted UGM samples in both analyses were assumed to be optimal (i.e. OMC and MDD), representing typical compaction conditions in road construction. It should be noted that precipitation events during both summer and winter periods were excluded from the microwave drying analysis, as construction and microwave dry-back processes are typically halted during rainy days in road construction practices.

The S_r variation over the depth of the compacted UGM samples under solar drying is shown in Fig. 15. Solar drying exhibited a strong dependency on seasonal climatic conditions. During summer, the target S_r of 60% was achieved in the surface layers after approximately 5 days of drying. In winter, drying was markedly slower, requiring 10–12 days for surface layers to approach the target S_r. During both periods, deeper layers retained higher S_r values, with less pronounced moisture gradients than the surface of the compacted UGM. Furthermore, Fig. 15 highlights that moisture removal during summer was concentrated near the surface due to high ambient

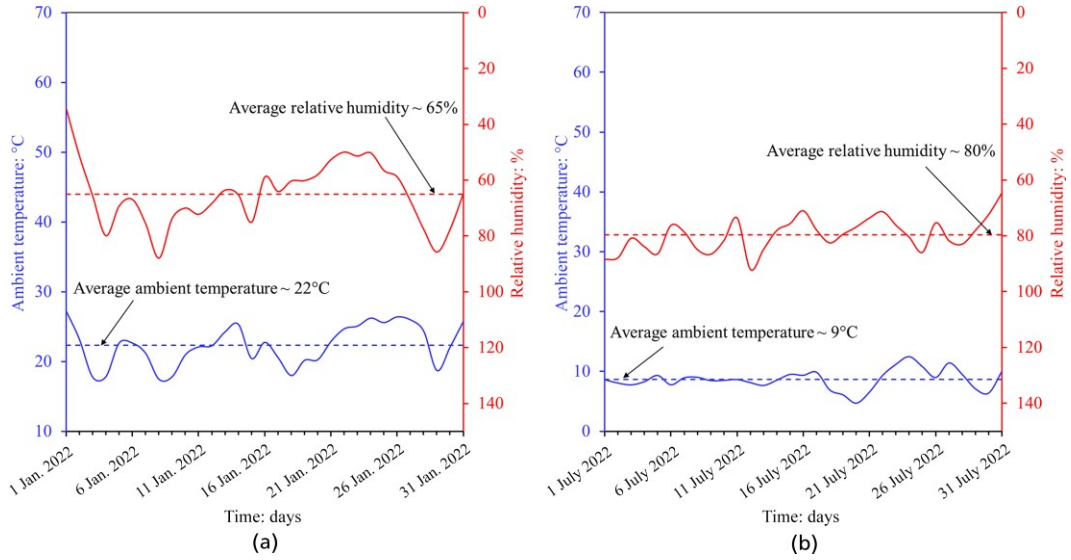

Fig. 13. Daily variations of ambient temperature and relative humidity with average values: (a) summer period; (b) winter period

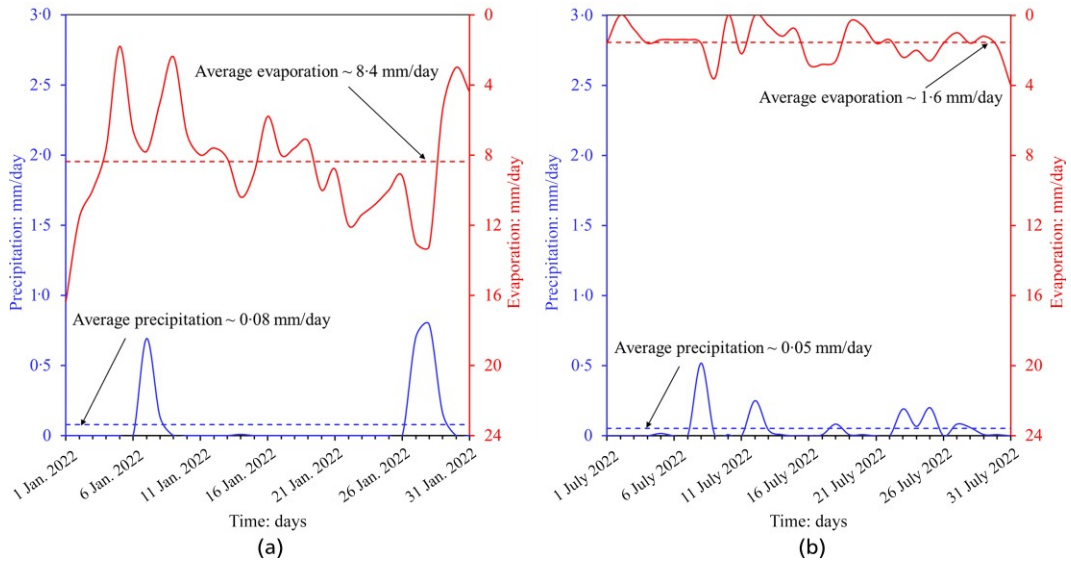

Fig. 14. Daily variations of precipitation and evaporation with average values: (a) summer period; (b) winter period

Downloaded from http://www.emerald.com/jgeot/article-pdf/76/4/579/11192475/jgeot.25.00085en.pdf by Monash University user on 08 June 2026

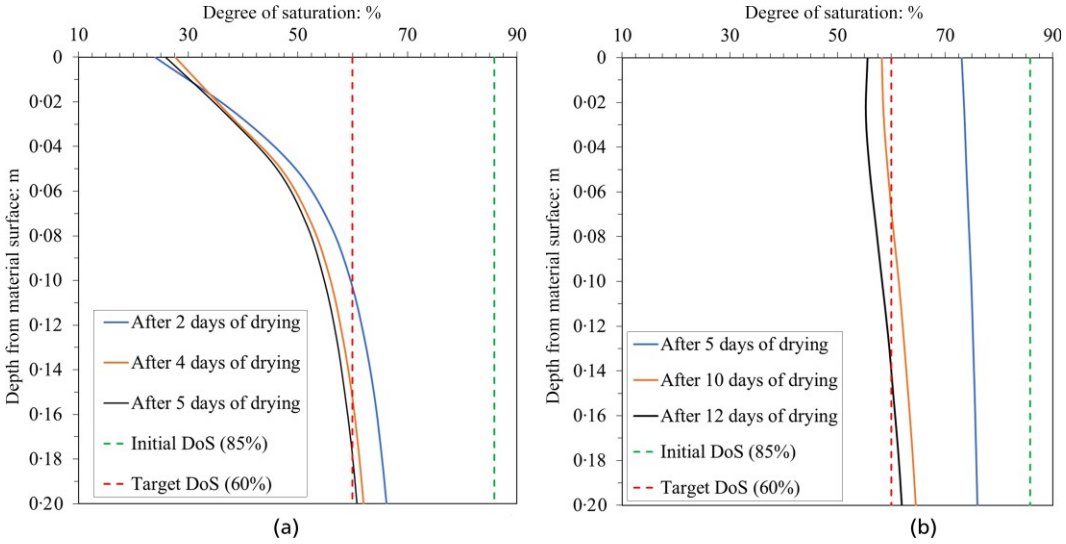

Fig. 15. S_r variation with depth under the solar drying process: (a) during summer; (b) during winter (DoS – Degree of Saturation)

temperatures and evaporation rates. During winter, lower ambient temperatures, higher relative humidity and reduced evaporation rates limited the drying performance, resulting in slower moisture migration and almost uniform moisture gradients across the depth.

The S_r profiles after microwave drying, conducted under both direct contact and gap conditions, are shown in Fig. 16. The drying duration for each condition was determined based on achieving the target S_r of 60%, with the direct contact condition reaching the target after 4 min, and the 1 cm gap condition after 5 min. Microwave drying demonstrated substantially faster drying than solar drying, with a notable reduction in S_r near the surface within a shorter time. Both summer and winter conditions yielded nearly identical results for both experimental conditions, indicating that microwave drying was generally independent of external climatic conditions. Moreover, the direct contact condition resulted in a steep surface gradient, achieving rapid near-surface drying but with limited penetration into deeper layers, whereas the gap condition produced a more uniform drying profile across depth but with slightly reduced efficiency due to lower energy transfer at the surface.

In terms of overall efficiency, microwave drying substantially outperformed solar drying, as described below.

(*a*) Solar drying required multiple days (e.g. around 5 days in summer, 10–12 days in winter) to achieve the target S_r of 60%.
(*b*) Microwave drying achieved near-surface drying to the target S_r in minutes (e.g. 4–5 min).
(*c*) Microwave drying demonstrated minimal dependence on climatic conditions, whereas solar drying was highly weather dependent despite being sustainable and cost effective. The effectiveness of solar drying was significantly influenced by temperature, humidity and evaporation rates, making it less practical for winter or humid environments.

However, microwave drying also presents challenges, as outlined below.

(*a*) Localised overheating was observed in laboratory experiments, posing potential safety risks. This would be a critical problem unless uniform microwave distribution can be achieved during field deployment.

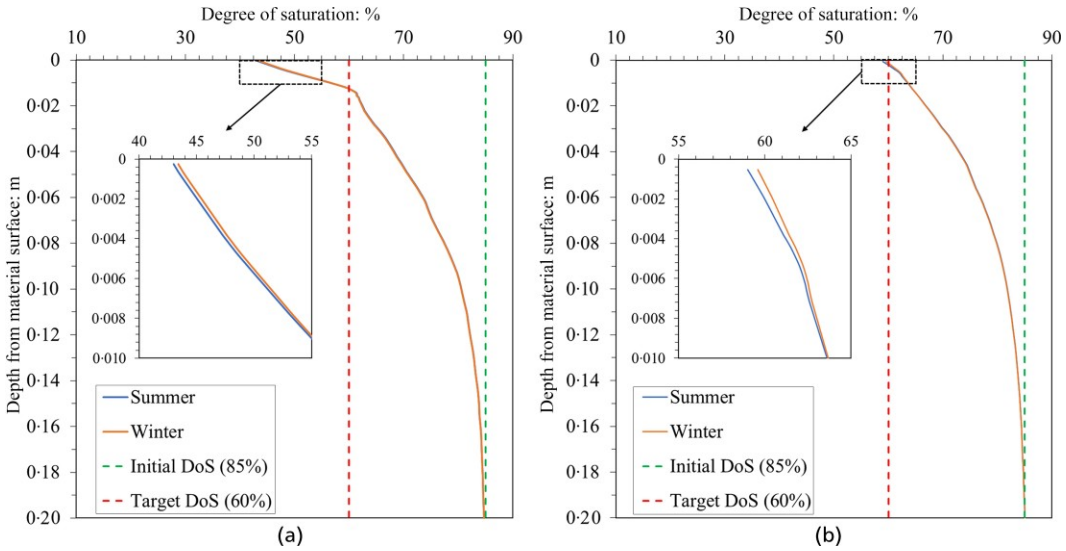

Fig. 16. S_r variation with depth under the microwave drying process: (a) direct contact condition (4 min of drying); (b) gap condition (5 min of drying) (DoS – Degree of Saturation)

Downloaded from http://www.emerald.com/jgeot/article-pdf/76/4/579/11192475/jgeot.25.00085en.pdf by Monash University user on 08 June 2026

(*b*) Energy penetration is limited, which reduced drying efficiency in deeper layers. However, both drying methods showed a non-uniform moisture removal over the depth of the compacted UGM sample, which was more pronounced when microwave drying. However, near-surface drying can be beneficial for asphalt sealing, where the adherence of the asphalt layer to the UGM surface can be enhanced for better performance.

(*c*) Several strategies may address these limitations in practice. Minimising the gap between the applicator and the compacted surface, for instance, using a lightweight wheel arrangement (Fig. 17(a)), can improve energy transfer while reducing exposure or leakage of microwave energy. Mounting the applicator on a moving vehicle (Fig. 17(b)) may reduce localised overheating by limiting exposure time at any given point, while repeated passes can promote more uniform drying across the treated surface. In addition, combining microwave energy with convective airflow could offer the potential to improve both drying uniformity and penetration depth. Such hybrid approaches may address the uneven moisture removal observed in laboratory tests and enhance the overall efficiency of field-scale applications. Future research will therefore focus on assessing these strategies, including moving microwave systems, multiple drying passes and microwave convective methods, to optimise dry-back performance in practice.

These findings can also be interpreted in the context of the state-based specifications summarised in Table 1. The rapid reduction in S_r near the surface to around 60% within minutes is consistent with the threshold requirements set by Queensland and the Northern Territory, and indicates potential alignment with the OMC-based limits adopted in other states (e.g. New South Wales, Western Australia, Victoria and South Australia). However, it is noted that the present results primarily demonstrate near-surface drying rather than uniform reduction across the full layer thickness. This suggests that while microwave drying shows promise for meeting practical sealing criteria, further optimisation is required to improve penetration depth and

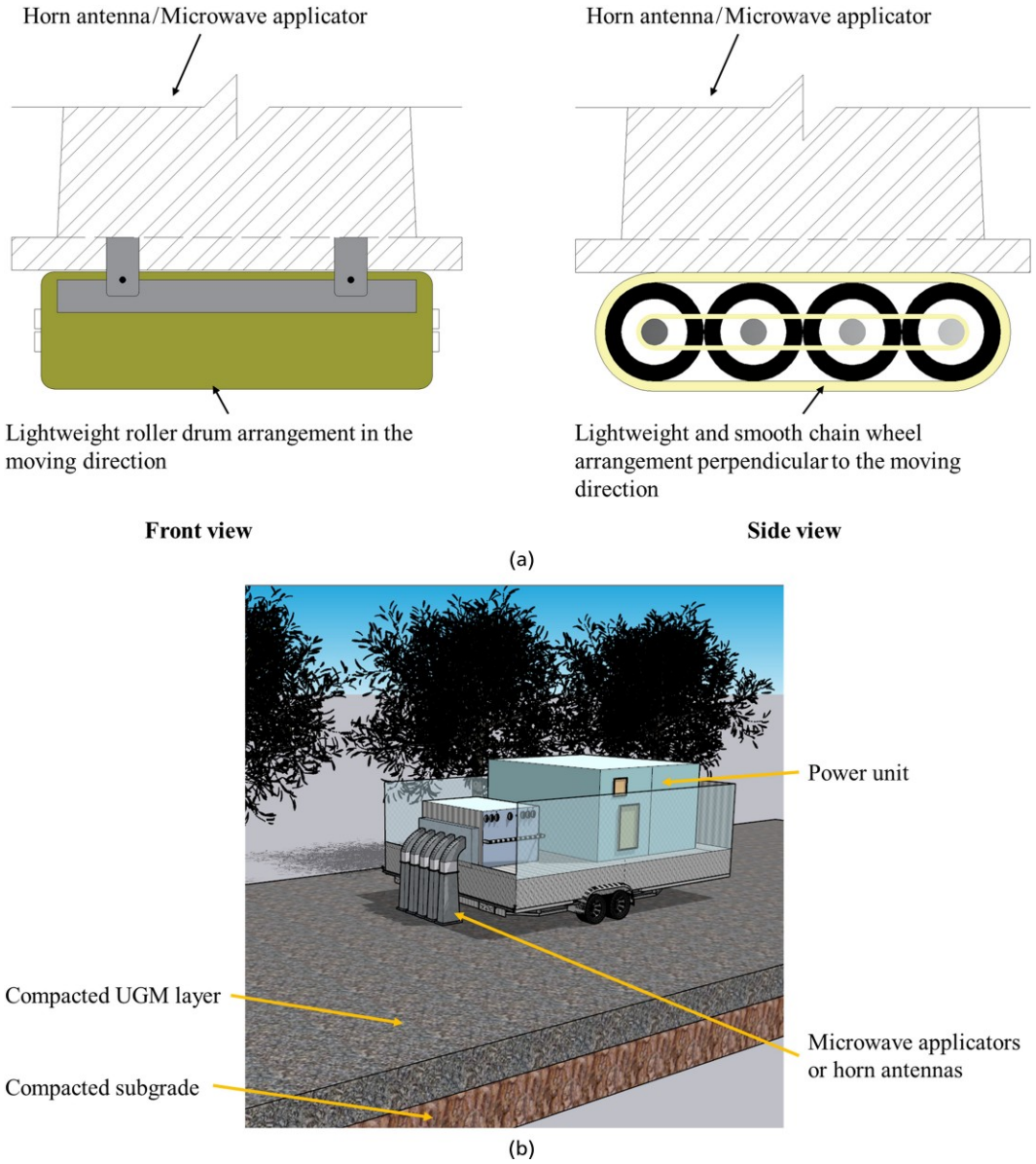

Fig. 17. Conceptual arrangements for field-optimised microwave drying: (a) lightweight wheel arrangement; (b) proposed vehicle-mounted microwave drying system (Athmarajah *et al.*, 2024)

Downloaded from http://www.emerald.com/jgeot/article-pdf/76/4/579/11192475/jgeot.25.00085en.pdf by Monash University user on 08 June 2026

ensure compliance with field-scale specifications. In addition to these technical challenges, field deployment of this technology would require careful attention to safety aspects, particularly to control potential microwave radiation leakage during field operation (e.g. electromagnetic shielding, on-site leakage monitoring systems, real-time temperature control and adherence to safety standards (Australian Radiation Protection & Safety Agency, 2002)).

CONCLUSIONS

This paper has investigated the effectiveness of microwave drying as an accelerated method to dry back compacted UGMs. The experimental and numerical investigations have demonstrated that the microwave dry-back process can expedite the drying of compacted granular pavement layers, potentially offering substantial time savings in pavement construction practices compared to the traditional dry-back process using solar radiation. The key findings of this study are as follows.

(*a*) The drying behaviour varies depending on the microwave applicator positioning:

  i. Direct contact with the UGM surface results in rapid surface moisture removal with limited energy penetration into deeper layers.
  ii. A 1 cm gap between the microwave applicator and the surface leads to a more uniform drying profile but slightly reduced efficiency due to energy dissipation.

(*b*) Numerical simulations agreed with experimental results, validating the finite-element model developed for capturing coupled heat and moisture transport phenomena during microwave drying.

(*c*) Microwave drying significantly accelerated near-surface moisture removal, achieving the target S_r within 4–5 min, compared to approximately 5 days in summer and 10–12 days in winter under solar drying.

(*d*) Microwave drying was mainly independent of external climatic conditions, whereas solar drying was highly sensitive to seasonal variations in temperature, humidity and evaporation rates.

(*e*) Practical considerations for field implementation include minimising the applicator-to-surface gap to maximise energy transfer efficiency while protecting the pavement surface. A lightweight rolling mechanism is proposed to maintain close contact between the microwave applicator and the compacted UGM layer.

(*f*) Challenges such as non-uniform drying and localised heating need to be addressed to improve the practical applicability of uniform microwave drying. Future research should explore microwave-assisted convective drying to enhance uniform moisture removal and mitigate potential thermal damage.

Overall, this study has established microwave drying as a viable and efficient alternative to conventional drying methods in pavement construction. Optimising microwave application techniques may potentially improve construction efficiency, reduce weather dependency and enhance the overall quality of compacted UGM in road infrastructure.

FUNDING

This research work was undertaken as part of a project (Project number: IH18.03.8) sponsored by the SPARC Hub (https://sparchub.org.au) at the Department of Civil and Environmental Engineering, Monash University, funded by the Australian Research Council (ARC) Industrial Transformation Research Hub (ITRH) Scheme (Project ID: IH180100010). The financial and in-kind support of EIC Activities of CIMIC Group and Monash University and the financial support of the ARC is acknowledged. The authors appreciate the technical support provided by the Department of Chemical and Biological Engineering at Monash University for measuring the specific heat capacity of the selected materials. Special thanks are also extended to Professor Graham Brodie for generously providing the microwave equipment used during the experimental work.

NOTATION

A	area of the dried region at the surface
a	length of the major axis
b	length of the minor axis
e	void ratio
G_s	specific gravity
h	depth
S_r	degree of saturation
V	total dried volume
w	gravimetric moisture content
ρ_d	dry density
ρ_w	density of water ($=1000\,kg/m^3$)

REFERENCES

Athmarajah, G. (2025). Microwave dry-back of granular pavement layers. PhD thesis, Monash University, Melbourne, Australia.

Athmarajah, G., Walker, J. P., Sounthararajah, A. & Kodikara, J. (2023). Influence of solar energy on the dry back process in road pavement construction: An experimental study. *XXVII PIARC World Road Congress*, 11.

Athmarajah, G., Sounthararajah, A., Walker, J. P., Deo, R. & Kodikara, J. (2024). An alternative technology using microwaves for dry back process of unbound granular pavements during construction – a review. *Transp. Geotech.* **46**, 101245.

Athmarajah, G., Walker, J., Kishore, K., Tophel, A. & Kodikara, J. (2025). Dielectric properties of class 2 UGM under varying moisture and temperature at 2.45 GHz for microwave dry-back modelling. *Geotechnical and Geological Engineering* **44**, No. 1, 37, 10.1007/s10706-025-03557-6.

Australian Radiation Protection and Safety Agency (2002). *Maximum exposure levels to radiofrequency fields – 3 kHz to 300 GHz*. Australian Radiation Protection and Safety Agency.

Austroads (2008). *Guide to pavement technology part 4A: Granular base and subbase materials, AGPT04A-08* Sydney, NSW, Australia: Austroads Ltd.

Benedetto, A. & Calvi, A. (2013). A pilot study on microwave heating for production and recycling of road pavement materials. *Constr. Build. Mater.* **44**, 351–359.

Brodie, G. & Hollins, E. (2015). The effect of microwave treatment on ryegrass and wild radish plants and seeds. *Glob. J. Agric. Innov., Res. Dev.* **2**, 16–24.

Chen, L., Ghorbani, J., Dutta, T. T., Zhou, A., McCartney, J. S. & Kodikara, J. (2024). A new multi-surface plasticity model for cyclic hardening of unsaturated granular soils. *Comput. Geotech.* **173**, 106500.

Department of Infrastructure Planning and Logistics Northern Territory Government (2017). Standard specification for roadworks. Palmerston, NT, Australia: Department of Infrastructure, Planning and Logistics.

Department of State Growth Tasmanian Government (2014). R40 pavement base and subbase, Roadworks Specification. Hobart, Tasmania, Australia: Department of State Growth-Tasmanian Government.

Department of Transport and Main Roads Queensland (2021). MRTS05 – unbound pavements. Brisbane, Queensland,

Downloaded from http://www.emerald.com/jgeot/article-pdf/76/4/579/11192475/jgeot.25.00085en.pdf by Monash University user on 08 June 2026

Australia: Department of Transport and Main Roads Queensland.
Ding, L., Wang, X., Zhang, W., Wang, S., Zhao, J. & Li, Y. (2018). Microwave deicing efficiency: Study on the difference between microwave frequencies and road structure materials. *Appl. Sci.* **8**, No. 12, 2360.
Dutta, T. T. & Kodikara, J. (2022). Evaluation of unbound/subgrade material rutting and resilient behaviour based on initial density and saturation degree. *Transp. Geotech.* **35**, 100782.
Flores, G., Gallego, J., Giuliani, F. & Autelitano, F. (2018). Aging of asphalt binder in hot pavement rehabilitation. *Constr. Build. Mater.* **187**, 214–219.
Florida Department of Transportation. (2021). Standard specifications for road and bridge construction. Tallahassee, FL, USA: Florida Department of Transportation.
Gao, J., Sha, A., Wang, Z., Tong, Z. & Liu, Z. (2017). Utilization of steel slag as aggregate in asphalt mixtures for microwave deicing. *J. Clean. Prod.* **152**, 429–442.
Gulisano, F. & Gallego, J. (2021). Microwave heating of asphalt paving materials: Principles, current status and next steps. *Constr. Build. Mater.* **278**, 121993.
Guo, L., Liu, C., Srinivasakannan, C. & Jiyun, G. (2021). Microwave upgradation of Yunnan lignite: dielectric properties, drying pattern and kinetics. *J. Microw. Power Electromagn. Energy* **55**, No. 3, 248–269.
Hefer, A. & Scullion, T. (2005). *Materials, specifications, and construction techniques for heavy-duty flexible bases: Literature review and status report on experimental sections*. Bryan, TX, USA: Texas Transportation Institute.
Jahangir, M. H. & Sadrnejad, S. A. (2013). A new coupled heat, moisture and air transfer model in unsaturated soil. *J. Mech. Sci. Technol.* **26**, No. 11, 3661–3672.
Khan, M. J., Brodie, G. I., Gupta, D. & Foletta, S. (2018). Microwave soil treatment improves weed management in Australian dryland wheat. *Trans. ASABE* **61**, No. 2, 671–680.
Li, H., Shi, S., Lin, B., Lu, J., Lu, Y., Ye, Q., Wang, Z., Hong, Y. & Zhu, X. (2019). A fully coupled electromagnetic, heat transfer and multiphase porous media model for microwave heating of coal. *Fuel Process. Technol.* **189**, 49–61.
Main Roads Western Australia (2021). Specification 501 – Pavements Western Australia. East Perth, WA, Australia: Main Roads Western Australia.
Midgley, L. (2010). *Technical Report TR 209: Best practice for the preparation of new granular pavement for thin bituminous surfacing*. VicRoads.
Norambuena-Contreras, J., Gonzalez, A., Concha, J. L., Gonzalez-Torre, I. & Schlangen, E. (2018). Effect of metallic waste addition on the electrical, thermophysical and microwave crack-healing properties of asphalt mixtures. *Constr. Build. Mater.* **187**, 1039–1050.
Standards Australia (2006). AS-1289.3.5.1: Methods of testing soils for engineering purposes – Soil classification tests – Determination of the soil particle density of a soil – Standard method. Sydney, Australia: Standards Australia.
Standards Australia (2009a). AS-1289.3.6.1: Methods of testing soils for engineering purposes – Soil classification tests – Determination of the particle size distribution of a soil – Standard method of analysis by sieving. Sydney, Australia: Standards Australia.
Standards Australia (2009b). AS-1289.3.1.1: Soil classification tests – Determination of the liquid limit of a soil: four point Casagrande method. Sydney, Australia: Standards Australia.
Standards Australia (2017). AS-1289.5.2.1: Methods of testing soils for engineering purposes: Soil compaction and density tests – Determination of the dry density/moisture content relation of a soil using modified compactive effort. Sydney, Australia: Standards Australia.
Texas Department of Transportation (2004). Standard specifications for construction and maintenance for highways: Streets and bridges. Austin, TX, USA: Texas Department of Transportation.
Tophel, A., Walker, J. P., Dutta, T. T. & Kodikara, J. (2022). Theory-guided machine learning to predict density evolution of sand dynamically compacted under K_0 condition. *Acta Geotech.* **17**, No. 8, 3479–3497.
Transport for NSW (2020). QA specification R71. Transport for NSW.
VicRoads (2017). Code of Practice RC 500.02 – Registration of crushed rock mixes, vol. **9**: VicRoads.
Zhang, F., Wang, D., Cannone Falchetto, A. & Cao, Y. (2024). Microwave deicing properties and carbon emissions assessment of asphalt mixtures containing steel slag towards resource conservation and waste reuse. *Sci. Total Environ.* **912**, 169189.

Downloaded from http://www.emerald.com/jgeot/article-pdf/76/4/579/11192475/jgeot.25.00085en.pdf by Monash University user on 08 June 2026